The miR166–SlHB15A regulatory module controls ovule development and parthenocarpic fruit set under adverse temperatures in tomato

Christian Clepet, Ravi Sureshbhai Devani, Rachid Boumlik, Yanwei Hao, Halima Morin, Fabien Marcel, Marion Verdenaud, Brahim Mania, Gwilherm Brisou, Sylvie Citerne, et al.

TITLE

The *miR166- SlHB15A* Regulatory Module controls Ovule Development and Parthenocarpic Fruit Set under Adverse Temperatures in Tomato

AUTHORS

Christian Clepet[1], Ravi Sureshbhai Devani[1], Rachid Boumlik[1], Yanwei Hao[1]†, Halima Morin[1], Fabien Marcel[1], Marion Verdenaud[1], Brahim Mania[1], Gwilherm Brisou[1], Sylvie Citerne[4], Gregory Mouille[4], Jean-Christophe Lepeltier[2], Shai Koussevitzky[3], Adnane Boualem[1] and Abdelhafid Bendahmane[1*]

AFFILIATIONS

[1]Institute of Plant Sciences Paris-Saclay, INRAE, CNRS, Université Paris-Saclay, Orsay 91405, France

[2]HM Clause, Mas Saint-Pierre, quartier La Galine, Saint-Rémy de Provence 13210, France

[3]Hazera Seeds Ltd, Berurim M.P. Shikmim 7983700, Israel

[4]Institut Jean-Pierre Bourgin, INRAE, Versailles, France.

CURRENT ADDRESS

†Key Laboratory of Horticultural Crop Biology and Germplasm Innovation in South China, College of Horticulture, South China Agricultural University, Guangzhou 510642, China.

RUNNING TITLE

miR166 and *SlHB15A* control ovule and fruit set

SHORT SUMMARY

Tomato fruit set is inhibited by adverse temperatures. The authors isolated *SlHB15A* loss-of-function mutants, leading to parthenocarpic fruit set under optimal and non-permissive temperatures. Under cold stress, *SlHB15A* is subjected to gene dosage regulation controlled

by *miR166*. SlHB15A acts as a bifunctional transcription factor, modulating auxin and ethylene signaling to interfere with fruit set in the absence of fertilization.

CONTACT

*Correspondence to: mailto: abdelhafid.bendahmane@inrae.fr

ABSTRACT

Fruit set is inhibited by adverse temperatures, with consequences on yield. We isolated a tomato mutant producing fruits under non-permissive hot temperatures and identified the causal gene as *SlHB15A*, belonging to class-III homeodomain leucine-zipper transcription factors (HD-ZipIII). *SlHB15A* loss-of-function mutants display aberrant ovule development that mimics transcriptional changes occurring in fertilized ovules and leads to parthenocarpic fruit set under optimal and non-permissive temperatures, in field and glasshouse conditions. Under cold growing condition, *SlHB15A* is subjected to conditional haploinsufficiency and recessive dosage sensitivity controlled by microRNA 166 (*miR166)*. Knockdown of *SlHB15A* alleles by *miR166* leads to a continuum of aberrant ovules correlating with parthenocarpic fruit set. Consistent with this, plants harboring *SlHB15A-miRNA166* resistant allele developed normal ovules and were unable to set parthenocarpic fruit under cold condition. DNA affinity purification sequencing (DAP-seq) and RNAseq analyses revealed SlHB15A is a bifunctional transcription factor, expressing in the ovule integument. SlHB15A binds to the promoters of auxin genes to repress auxin signaling and to ethylene genes to activate their expression. Survey of tomato genetic biodiversity identified *pat* and *pat-1*, two historical parthenocarpic mutants, as alleles of *SlHB15A*. Our finding demonstrates the role of *SlHB15A* as a sentinel to prevent fruit set in the absence of fertilization and provides a mean to enhance fruiting under extreme temperatures.

KEYWORDS: Parthenocarpy; Dosage sensitivity; HD-ZipIII; miRNA166; Heat stress; Cold stress.

INTRODUCTION

In flowering plants, ovules are seed precursors made up of one or two sheathing integuments surrounding a nucellus in which meiosis, fertilization and embryo development occur (Cooper, 1931). Ovule, seed and fruit development are tightly coordinated. At anthesis the ovary stops cell divisions and enters a growth-arrest phase, or resumes cell division to develop into a fruit when pollinated (Joldersma and Liu, 2018). Fruit can develop independently of ovule fertilization in a process referred to as parthenocarpy. This alternative pathway can be genetically controlled or artificially induced by phytohormones (Joldersma and Liu, 2018).

Reproductive organs are highly sensitive to environmental factors. In particular, heat stress affects anthers development, style elongation, meiosis, pollen release, pollen germination pollen-tube growth, pollen/pistil interaction, fertilization, endosperm formation and embryo development, with consequences on fruit set (*e.g.* Abdul-Baki and Stommel, 1995; Sato et al., 2000; Erickson and Markhart, 2002; Firon et al., 2006; Zinn et al., 2010; Giorno et al., 2013). On average, global yields will fall by 3 to 7.4% for each degree-Celsius increase (Zhao et al., 2017a). Cold stress also severely hampers the development of reproductive organs, causing severe necrosis, homeotic-floral transformations and poor pollen germination (Zinn et al., 2010). Improving flower fertilization and fruit set under a wider range of temperatures can help achieve year-round cropping and more importantly, maintain a sustainable agriculture in the scenario of a 2-to-4-°C increase, projected for 2100 (Zhao et al., 2017a).

In tomato (*Solanum lycopersicum*) the fruit set is strongly hindered at temperatures above 29 °C (Peet et al., 1998) or lower than 12.8 °C (Charles and Harris, 1972). Because of these limitations, tomato cultivation is restricted to certain geographic areas and time of the year (Joldersma and Liu, 2018). Tomato fruit set relies on a complex regulation involving positive and negative growth factors. Notably the pollination induces a burst of auxin and gibberellin (GA) biosynthesis and as suggested by various studies, auxin promotes ovary growth at least partially by increasing GA synthesis (Serrani et al., 2008; Dorcey et al., 2009). More recently the gaseous hormone ethylene was proposed to connect auxin and GA, preventing GA perception and fruit set (Shinozaki et al., 2018). The ovule has a predominant role in this developmental program, the burst of auxin and GA is mainly produced by the young embryo or surrounding tissue (Dorcey et al., 2009; Pattison et al., 2015; Zhang et al., 2016), whereas in the absence of fertilization, ethylene is produced, promoting ovule senescence and flower drop (Carbonell-Bejerano et al., 2011). These knowledges were drawn in part from the

knockdown of the *AUXIN RESPONSE FACTOR 7* (*ARF7*) (de Jong et al., 2009b) or *DELLA* (Marti et al., 2007), or by inducing the expression of auxin (Rotino et al., 1997) or GA biosynthesis enzymes (Garcia-Hurtado et al., 2012). Together with hormones, gene regulatory networks are recruited to control fruit set. This includes transcription factors post-transcriptionally modulated by microRNAs (miRNAs; Jones-Rhoades *et al*., 2006). For instance, tomato lines overexpressing *miR167,* targeting ARF6/8 are unable to generate fruits (Liu *et al*., 2014). In contrast tomato lines overexpressing *miR159,* targeting *GAMYB1/2* display obligatory parthenocarpy (da Silva *et al*., 2017). Nevertheless, the mechanisms through which unfertilized ovules interfere with fruit development are still poorly characterized. We report a new regulatory module, in which *miR166* and *SlHB15A* control ovule development and fruit set in tomato. *SlHB15A*-loss-of-function mutants exhibit aberrant ovules and parthenocarpic fruits under adverse temperature conditions. *SlHB15A* is also dosage sensitive under cold conditions. We demonstrate that this process implicates the cold induction of *miR166*, knocking down *SlHB15A*, and consequently leading to fruit set. Transcriptome analysis as well as genome-wide identification of SlHB15A-direct targets showed SlHB15A acts as a bifunctional transcription factor, modulating auxin and ethylene signaling to interfere with fruit set in the absence of fertilization.

RESULTS

Pf1 Mutant Produces Fruits under Non-Permissive Hot Conditions

Although tomato can grow in wide range of environments, the reproductive phase is highly sensitive to non-optimal low and high temperatures (Charles and Harris, 1972; Peet et al., 1998; Zinn et al., 2010). To identify fertilization-independent fruit set, we screened an Ethyl Methanesulfonate (EMS)-mutagenesis population under non-permissive-heat conditions. One mutant line, named hereafter parthenocarpic fruit 1 (*pf1*), set seedless fruits and was further investigated in an insect-proof and temperature-controlled greenhouse. Following stamen ablation, flowers in *pf1* line developed into seedless fruits while flowers of M82-parental line showed no fruit set (Figure 1A to 1H). Extended phenotyping of *pf1* fruits revealed no obvious developmental phenotypes but the fruits were smaller, and more abundant (Supplemental Figure 1). Some of the ripe fruits displayed malformations (Supplemental Figure 1H, 1K and 1M) but these defects were not seen when *pf1* was introgressed in medium-fruited and cherry-sized round-tomato cultivars, likely due to interaction with fruit-

shape genes (Rodriguez et al., 2011) (Figure 1E to 1H and Supplemental Figure 1B). Synchronous fruit set and ripening are key traits in processing-tomato breeding. Interestingly, *pf1* produced twice the amount of ripe fruits at harvest than the wildtype (Supplemental Figure 1J, 1L and 1M and Supplemental Text), likely because of the fertilization that is not required. Further phenotyping of vegetative and flowering traits are discussed in Supplemental Text and Supplemental Figure 2.

In addition to high temperatures, hot nights and small differences between night and day temperatures are well known to interfere with fruit set. We tested whether *pf1* allele confers fruiting advantage at 32 °C/ 24 °C day/ night, non-permissive conditions. In contrast to wildtype, *pf1* plants were able to set fruits (Figure 1I to 1P).

pf1 is Mutated in an HD-ZipIII Transcription Factor

Backcrossing and segregation analysis identified *pf1* as a single-locus-recessive mutation (Supplemental Figure 1A). To identify the causal mutation, we sequenced bulked-genomic DNA from parthenocarpic and non-parthenocarpic M2 plants and determined the delta-SNP index (Figure 1Q, 1R and Supplemental Figure 3). Fine mapping further delimited *pf1* to a single gene, *SolyC03g120910*, harboring an EMS-induced G3872A transition. This one-base transition leads to a premature stop codon, W411*, suggesting that *pf1* is a null allele. Protein alignment and phylogenetic analysis revealed that *SolyC03g120910* encodes an HD-ZipIII protein, named hereafter *SlHB15A*, in reference to *AtHB15*, the closest homolog in *Arabidopsis thaliana* (Supplemental Figure 4A and 4B) and the nomenclature of HD-ZipIII proteins (Xu et al., 2019).

To confirm the role of *SlHB15A* in fruit set, we screened the gene for induced mutations, using Targeting Induced Local Lesions in Genomes (TILLING) and Clustered Regularly Interspaced Short Palindromic Repeats (CRISPR)-Cas9 (CRISPR-Cas9) approaches. Out of 62 alleles we isolated (Supplemental Table 1), 26 were predicted to induce changes in the amino-acid sequence and were backcrossed to wildtype. Segregant plants were then phenotyped for fruit set. As expected, plants homozygous for non-sense, splicing, deletion or deleterious-missense mutations were parthenocarpic (Supplemental Figure 5), validating the role of *SlHB15A* in inhibition of fruit set in the absence of fertilization.

To assess the level of polymorphism at *SlHB15A*, we examined the sequence diversity of the coding region in a panel of 401 accessions that includes 9 lines previously described as

parthenocarpic or seedless. We identified 5 gene variants, leading to 4 missenses and one codon deletion (Supplemental Table 2). Three missense mutations, C561G, L712S and P805L, were predicted to not impact the function of the protein and plants harboring these mutations did not set fruits in the absence of pollination. Interestingly, two other mutations, a G583R missense and an A567 deletion, were revealed respectively in two accessions, *pat* (Soressi and Salamini, 1975) and *pat-1* (Pecaut and Philouze, 1978), previously described as parthenocarpic (Supplemental Table 3). Next, we crossed *pat* and *pat-1* to *pf1* to test if they are allelic. For each cross at least 10 F1 plants, and 10 manually castrated flowers per plant, were phenotyped for parthenocarpic fruit set. We found all F1-hybrid plants were parthenocarpic, confirming that *pat*, *pat-1* and *pf1* are all alleles of *SlHB15A*.

SlHB15A-Hypomorphic Alleles Lead to Parthenocarpy under Cold-Growing Conditions

Although low temperatures are a prerequisite for floral induction in many species (Xu and Chong, 2018), cold stress is a devastating factor for fruit set (Charles and Harris, 1972). To test whether *SlHB15A* alleles can confer fruiting advantage under cold growing conditions, plants were grown at 15 °C day/ 12 °C night (cold stress) and phenotyped for fruit set. These unfavorable conditions decreased the fruit set by ~60% in wildtype-pollinated-control plants, while *SlHB15A*-loss-of-function mutants were not affected (Figure 2A to 2H). We even observed an increase in fruit set of up to 70% in *pf1* plants, compared to control plants (Figure 2I). Unexpectedly, plants harboring loss-of-function mutations, at a heterozygous state, were found parthenocarpic, suggesting that *SlHB15A* is haploinsufficient to inhibit fruit set under cold stress (Figure 2E and Supplemental Figure 6A). To test whether this cold-induced parthenocarpy also occurs in field-growing condition, we cultivated 4 *SlHB15A* mutants, *pf1, pf1-4, pf1-17* and *pf1-20* showing recessive parthenocarpy under optimal temperature, in winter over two seasons (Supplemental Figure 6C to 6E). As for plants grown in glasshouse conditions, all four heterozygous mutants were parthenocarpic during winter cultivation. Unlike *pf1* homozygotes, parthenocarpic fruits of *pf1* heterozygote plants were similar in size to fruits of wildtype plants grown under optimal conditions, and did not show any malformation (Figure 2G, 2H and Supplemental Figure 6B).

The sensitivity of *SlHB15A* to gene dosage suggests that hypomorphic alleles, such as N92Y (*pf1-3*), may still lead to parthenocarpy under cold growing conditions. The N92Y mutation is

located in the leucine-zipper domain, predicted to be required for SlHB15A dimerization, still plants homozygous for the N92Y mutation are not parthenocarpic under optimal or hot conditions (Supplemental Figure 5). Under cold growing conditions, the N92Y mutant was found parthenocarpic only at homozygous state, and *pf1/pf1-3*-compound heterozygotes exhibited strong induced parthenocarpy (Figure 2J to 2Q), in line with *pf1*-heterozygous mutant phenotype. *pf1/pf1-3* hybrids were never scored as parthenocarpic under optimal or hot conditions (Supplemental Table 4). Consistent with this, two other hypomorphic alleles, *pf1-2* and *pf1-16*, non-parthenocarpic under hot and control conditions (Supplementary table 4) were found parthenocarpic in the winter field test (Supplemental Figure 6F). We refer to this cold-induced parthenocarpy as conditional parthenocarpy (Supplemental text).

miR166 is a Cold-Inducible Switch of Parthenocarpy in Tomato

Next, we investigated if this gene-dosage effect was dependent on *SlHB15A* mRNA accumulation under cold stress. Thus, we analyzed *SlHB15A*-expression pattern in developing flowers, from stage 1 to 4 days post anthesis, as well as in leaf and shoot apex. We found uniform and ubiquitous accumulation, using quantitative polymerase chain reaction (qPCR) (Figure 3A and Supplemental Figure 7A). However spatial-expression analysis using *in-situ* hybridization pinpointed to localized accumulations. *SlHB15A* mRNA was detected in shoot-apical meristem, sympodial meristem and vascular elements. The strongest expression was detected in transition meristem, inflorescence meristem and flower-meristem dome (Figure 3K to 3N and Supplemental Figure 7B to 7D). Expression was also observed in ovule primordia and in the outer cell layer of the ovule integument (Figure 3O, 3P and Supplemental Figure 7E).

As mRNA accumulation of HD-ZipIII transcription factors are known to be controlled by *miR166s* (Kim et al., 2005), we analyzed tomato-reproductive-organ degradomes (Lopez-Gomollon et al., 2012) and revealed *SlHB15A*-cleavage site matching *miR166* pairing (Figure 3B). Because *miR166* was reported to control development (Hashimoto et al., 2018) and modulate plant responses to abiotic stresses including low temperature (Omidvar et al., 2015), we investigated whether *miR166* controls conditional parthenocarpy under cold growing conditions. Using *in-situ*-hybridization, we revealed overlapping expression of *miR166* and *SlHB15A* in a range of tissues, including sympodial, inflorescence and flower meristems, as well as developing flowers (Figure 3C, 3D, 3K, 3L and Supplemental Figure 7). qPCR

analysis revealed cold-induced expression of *miR166* (Figure 3Q) but failed to show reproducible down accumulation of *SlHB15A* mRNA under cold conditions (Supplemental Text and Supplemental Figure 7M). We therefore used genetics to demonstrate that *miR166* is the cold-inducible switch of *SlHB15A*-dosage sensitivity. In order to not alter the expression of *SlHB15A*, we used TILLING to screen for *SlHB15A* miR166-resistant allele. We isolated a line, *pf1-6,* harboring a C2672T substitution that disrupts the complementarity with *miR166* (Figure 3B, Supplemental Figures 5 and 8A to 8J). Even though C2672T is a non-synonymous mutation, it leads to a conserved mutation that does not confer parthenocarpy at any condition (Figure 3G and 3H). In line with *pf1-6* is a *miR166*-resistant allele, *pf1-6*-homozygous mutant displayed no mRNA down-accumulation, concurrently with the *miR166* induction and a *miR166*-resistant mutation identical to *pf1-6* was described in another HD-ZipIII transcription factor, *Oryza sativa* lateral floret 1 (*OsLF1)* (Zhang et al., 2017) (Figure 3Q, Supplemental Figure 8B and Supplemental Text). By crossing *pf1-6/pf1-6* and *pf1/pf1* homozygotes, we generated compound-heterozygote *pf1/pf1-6* plants that we phenotyped for parthenocarpy under cold conditions (Figure 3E to 3J and Supplemental Figure 8K). All hybrid plants did not set fruits in the absence of fertilization (Figure 3S), validating genetically that *miR166* is the cold-inducible switch leading to parthenocarpy. To further demonstrate the down accumulation of *SlHB15A* mRNA under cold conditions, we took advantage of *PF1/pf1-6* heterozygote plants. We predicted that even small and transient induction of *miR166* under cold conditions should lead to measurable differences in the relative accumulation of mRNAs from the two alleles. The difference should be also exaggerated under cold stress. Thus, we conducted a comparative transcriptomic analysis of flowers of *PF1/pf1-6* heterozygote plants grown under cold stress or control conditions (Supplemental text). We found *pf1-6* mRNA accumulating on average 1.5 fold more than *SlHB15A* mRNA, under cold stress, confirming that *pf1-6* is indeed *miR166*-resistant. These data also demonstrate that the cold stress leads to the down accumulation of *SlHB15A* mRNA (Figure 3R). Collectively, these data demonstrate that *miR166* is likely the cold-inducible switch leading to *SlHB15A*-dosage sensitivity and parthenocarpy.

A Gradient of Aberrant Ovules Correlates with Parthenocarpy

As *SlHB15A* is highly expressed in ovule integument, we examined the ovules of *SlHB15A* mutants. Prior to integument initiation at stage 11, no visible ovule alteration was observed

(Supplemental Figure 9A and 9B). In contrast, at stage 18 and 20, most *pf1* ovules are orthotropous and the integument is aborted, remaining at the base of the nucellus (Figure 4A to 4C, Supplemental Figure 9G, and Supplemental Text). In line with the lack of integument in aberrant ovules, the integument-marker gene, *INNER NO OUTER* (*INO*) (Skinner et al., 2016), was not expressed in *pf1* dissected ovules (Supplemental Figure 9U). Ovule defects have been correlated with parthenocarpy in tomato, however whether defective ovules are the cause of the parthenocarpy remained an open question (da Silva et al., 2017; Hao et al., 2017; Wang et al., 2009). We exploited the conditional-*SlHB15A* parthenocarpy to assess the extent to which aberrant ovules correlate with parthenocarpy. Plants, harboring different *SlHB15A*-allelic combinations were cultivated in optimal and cold growing conditions and phenotyped for aberrant ovules development. We found less than 1% of aborted ovules in WT plants. In contrast, *pf1/pf1*-homozygous plants exhibited 91% of aberrant ovules at 25 °C and 95% under cold stress (Figure 4F, 4I, 4J and Supplemental Figure 9). *pf1/PF1* heterozygotes behaved like WT at 25 °C, but under cold condition more than 50% of the ovules were aberrant (Figure 4E, 4H, 4J and Supplemental Figure 9). Plants homozygous for *pf1-3* hypomorphic allele, showed no ovule phenotype at 25 °C and a small but significant number of aberrant ovules under cold stress (20%; Figure 4J and Supplemental Figure 9N and 9Q). *pf1/pf1-3* ovaries displayed only a few aberrant ovules at 25 °C (2.9%) whereas under cold, they harbored almost as many of those as *pf1/pf1* genotype (83%; Figure 4J and Supplemental Figure 9O and 9R). Since *pf1/pf1-6* plants harbored normal ovules in both conditions, we concluded that the *pf1-6 miR166*-resistant allele preserves against parthenocarpy as well as aberrant-ovule development under cold conditions (Figure 4J and Supplemental Figure 9L and 9P). Altogether, these data point to *miR166* inactivation of *SlHB15A* to a threshold leading to aberrant ovule development and consequently to parthenocarpy.

Aberrant Ovules Mimic Pollinated Ovules

SlARF7 is a key marker gene of flower fertilization, expressed in ovules at anthesis stage and downregulated after pollination (de Jong et al., 2009b). To analyze to which extent aberrant ovules behave like fertilized ovules, we measured the expression of *SlARF7* in *pf1* ovules and found downregulation like in wildtype fertilized ovules (Supplemental Figure 9S and 9V). To extend this analysis, we compared the transcriptome of *pf1* ovules to unfertilized wildtype ovules, which revealed 3391 differentially expressed genes (DEGs, 1879 upregulated and

1512 downregulated) (Supplemental Figure 10 and Supplemental Table 6). Then, the obtained DEGs were compared to the 851, 1979 and 3325 DEGs obtained in the comparison of fertilized *versus* un-fertilized wildtype ovules, collected at 1, 2 or 5 days post pollination (DPP) (Zhang et al., 2016), respectively. A strong transcriptome overlap increasing from 1 to 5 DPP, with a *P*-value close to zero at 5 DPP was obtained (Figure 5A and Supplemental Figure 10). Gene-Ontology (GO) analysis on shared DEGs revealed enrichment for GO terms related to signaling and response to auxin in the upregulated genes, and response to ethylene in the downregulated genes, in line with their role in fruit-set control (Figure 5B) (Joldersma and Liu, 2018). Additional enrichment was observed for cell cycle, microtubule-based process and polysaccharide metabolic process in the upregulated genes. In summary, the strong transcriptome overlap shows that *pf1* aberrant ovules mimic fertilized ovules and this likely implicates *SlHB15A* as a key-hormone regulator, repressing auxin and activating ethylene biosynthesis and signaling in ovules.

To test whether *SlHB15A* directly controls the auxin and the ethylene pathways in unfertilized ovules, we mapped genome-wide SlHB15A DNA binding, using DAPseq (Supplemental Table 7). A total of 14692 highly-reliable SlHB15A-binding sites, mostly in the 5' vicinity of the transcription-start site of 4254 unique genes, were identified (Figure 5C and Supplemental Figure 11). A consensus motif (*P*-value= $1e^{-6266}$) computed from >80% of these sequences, encompasses the binding site previously characterized by DAPseq for *Arabidopsis* AtHB15 (O'Malley et al., 2016) (Figure 5D) and *in planta*, by Chromatin Immunoprecipitation sequencing (ChIPseq) for the Arabidopsis-SlHB15A homolog, REVOLUTA (Brandt et al., 2012). We next integrated these data with our transcriptomic analysis and identified 270 and 202 genes that were both bound by SlHB15A and up- or downregulated in *pf1* ovules, respectively (Figure 5E). GO analysis further revealed strong enrichment of terms related to auxin biosynthesis, transport and signaling in the upregulated genes and ethylene biosynthesis and signaling in the downregulated genes, revealing the role of *SlHB15A* in repression of auxin and induction of ethylene pathways in unfertilized ovule (Supplemental Figure 11C). In particular, auxin biosynthesis genes, such as *TOMATO FLOOZY 2* (*ToFZY2)* and *ToFZY3,* were found bound by SlHB15A and upregulated in wildtype-fertilized and in *pf1* ovules (Figure 5F and Supplemental Figure 11D). Likewise, the auxin response factor *SlARF7* was found bound by SlHB15A and downregulated in wildtype-fertilized and in *pf1* ovules (Figure 5F and Supplemental Figure 9S and 9V). Conversely, the ethylene-biosynthesis and -signaling

genes, such as *1-AMINOCYCLOPROPANE-1-CARBOXYLIC ACID OXYDASE 4 (ACO4), ETHYLENE INSENSITIVE 3- LIKE 2 (EIL2*) and *ETHYLENE RESPONSE FACTOR 1* (*SlERF.1*) were found bound by SlHB15A and downregulated in fertilized and *pf1* ovules (Figure 5F and Supplemental Figure 11E). To validate the binding of SlHB15A to the identified auxin and ethylene genes, we used Electrophoretic Mobility Shift Assay (EMSA). SlHB15A protein was produced in *Escherichia coli*, in fusion to GST and incubated with biotin labelled cis-regulatory elements identified in DAP-seq. We tested the binding to two auxin biosynthesis genes, *ToFZY2* and *ToFZY3,* the auxin transporter*, PIN FORMED 4* (*SlPIN4*) and the auxin response factor *SlARF7.* For ethylene, we tested three ethylene response factors, *SlERF.F1, SlERF.B13* and *SlERF.H12.* Strong band shifts were obtained for all the probes and only when the biotin labeled probes were incubated with SlHB15A protein, and not with GST (Figure 5G and Supplemental Figure 11F). The band shift disappeared in a competition experiment with increased concentration of unlabeled probes (Figure 5G and Supplemental Figure 11F). To test whether the control of the expression of auxin and ethylene genes has consequences on hormone production, we measured auxin and ethylene in ovaries of *pf1* and control plants at 0, 2 and 4 days post anthesis (DAA). Consistent with ethylene negatively correlating with the progression of early fruit development, we found ethylene synthesized by pollinated *PF1* ovaries decreasing from 2 DAA and onwards (Figure 5I). Likewise, and consistent with early fruit development, we measured low level of ethylene from anthesis stage and onwards in *pf1* ovaries (Figure 5I). Consistent with auxin correlating with the progression of early fruit development, we found auxin synthesized by pollinated *PF1* ovaries increasing from 2 DAA, and *pf1* ovaries accumulating high concentration of auxin from anthesis and onwards (Figure 5H).

DISCUSSION

We isolated a mutant producing parthenocarpic fruits at non-permissive temperatures and identified the causal mutation in an HD-ZipIII transcription factor, *SlHB15A*. Based on a large spectrum of alleles, we could show that *SlHB15A* confers both obligate and conditional parthenocarpy in controlled and field conditions (Supplemental Text). At homozygous state, *SlHB15A* loss-of-function alleles, such as *pf1* or *pf1-4*, were found to lead to obligate parthenocarpy under optimal and non-permissive temperatures. At heterozygous state, the same alleles were found to lead to parthenocarpy only under cold growing conditions. We

also found that weak alleles, such as *pf1-3* and *pf1-16,* lead to parthenocarpy only at the homozygous state and under non-permissive cold conditions. Later, we demonstrated using *SlHB15A-miR166* resistant line that this conditional parthenocarpy is controlled by the cold induction of *miR166*, knocking down *SlHB15A* transcript. *pf1-3* harbors a missense mutation in a highly-conserved leucine-zipper residue which could partially affect the function of the protein. In line with this, we could evidence that under optimal temperature, this hypomorphic allele confers a weak ovule phenotype in the context of the strong *pf1* allele (Figure 4, Supplemental Figures 9 and 12). We explain these phenotypes by conditional gene-dosage effects. Whereas the haploinsufficiency of the strong alleles (pf1, pf1-4, pf1-17, pf1-20) is likely due only to the limiting amount of the transcript translated into wildtype protein, the dosage sensitivity of *pf1-3* , pf1-16 and pf1-2 should be accounted for by both the altered protein function and the amount of transcript (Supplemental Figures 6 and 12).

Developmental processes are often controlled by tightly-regulated dosage-sensitive genes (Johnson et al., 2019). Likewise, several genes involved in the development of the seed integument have already been associated with gene-dosage effects (Pillitteri et al., 2007; Wang et al., 2008; Zhao et al., 2017b). Conditional haploinsufficiency was also shown in yeast, in response to growth-medium composition (Deutschbauer et al., 2005). Yet, to our knowledge the *miR166-SlHB15A* genetic system is the first report of conditional haploinsufficiency and recessive dosage sensitivity controlled by a microRNA.

SlHB15A loss of function mutants display aberrant ovules with aborted integument remaining at the base of the nucellus. In *Arabidopsis*, the development of the integument is also controlled by HD-ZipIII transcription factors, evidenced in the triple mutant *corona* (*cna*), *phabulosa* (*phb*) and *phavoluta* (*phv*) (Kelley et al., 2009). Systematic phenotyping of *SlHB15A* mutant plants under optimal or adverse temperature conditions revealed a gradient of 2% - 95% defective ovules per ovary. Ovule defects were previously reported in other parthenocarpic mutants of tomato, such as the *INDOLE-3-ACETIC ACID 9* (*IAA9*) silencing line where growth of integument is affected (Wang et al., 2009), the *miR159-GAMYB1/2* transgenic system which displays abnormal growth of the embryo sac (da Silva et al., 2017), or the *SPOROCYTELESS/NOZZLE* (*SPL/NZZ)* deletion mutant which develops incomplete ovules lacking integument and megaspore mother cell (Hao et al., 2017). In our case, by exploiting the cold-inducible parthenocarpy, we could demonstrate that defective ovules fully correlate with parthenocarpy. This is intriguing, pointing towards the role of *SlHB15A* and the

integument in inhibiting the initiation of fruit set until fertilization. This also opens the question how the fertilization relieves the carpel from *SlHB15A*-mediated inhibition.

We found by transcriptome profiling that *pf1*-aberrant ovules behave similarly to wildtype-pollinated ovules. Notably they share different members of gene families associated with the biosynthesis or signaling of auxin and ethylene hormones (Zhang et al., 2016; Joldersma and Liu, 2018). Cis-regulatory elements and expression analyses further revealed SlHB15A is a bifunctional transcription factor. We show that SlHB15A binds to a DNA motif, matching the consensus binding site previously described for AtHB15 (O'Malley et al., 2016) and another HD-ZIPIII transcription factor (Brandt et al., 2012). We found several auxin genes to be targeted by SlHB15A and differentially expressed, notably, two YUCCA-like flavin monooxygenases, *ToFZY2* and *ToFZY3,* are upregulated in fertilized flowers and in *pf1* loss-of-function mutants, consistent with auxin-biosynthesis transgenes leading to parthenocarpy (Rotino et al., 1997). We also found *SlARF7* targeted and downregulated in *pf1* ovules, also in line with the knockdown of *SlARF7* leading to parthencarpy (de Jong et al., 2009b). In accordance with SlHB15A repressing auxin biosynthesis genes, we found the levels of auxin in *pf1* ovaries, at anthesis stage, similar to the level of auxin in wildtype ovaries 2 DPP. Besides auxin, we found *pf1* ovaries releasing low amounts of ethylene, and ethylene response factors, especially *SlERF.F1*, *SlERF.B13* and *SlERF.H12,* targeted by SlHB15A and downregulated in *pf1* ovules, also consistent with ethylene acting as a negative fruit-set regulator (Shinozaki et al., 2018).

In *Arabidopsis*, the lack of integument in *ats-1* mutant was associated with over accumulation of GA (Gomez et al., 2016). To test whether the lack of integument in *SlHB15A* loss-of-function mutants is due to a GA accumulation, we analyzed the expression of *GA20 oxidase1 (SlGA20ox1)* and the integument marker gene, *INO*. *SlGA20ox1* is a key GA-biosynthesis gene induced following flower fertilization (Serrani et al., 2007; Okabe et al., 2019). Interestingly, we found a ~2-fold-increased expression for *GA20ox1* in *pf1* flower from stage 11 and onwards (Supplemental Figure 13A), when integument initiation normally takes place (See *INO* expression, Supplemental Figure 13B). We also found the expression of *SlGA20ox1* upregulated in *pf1*-aberrant ovules and in dissected-ovules plus placenta (Supplemental Figure 9T and 9V).

During the submission of this work, Shinozaki and colleagues reported on the role of tomato *DELLA* homolog called *PROCERA* and its loss-of-function mutant, *procera* (*pro*) in

parthenocarpic fruit set (Shinozaki et al., 2020). Interestingly *SlHB15A* was found to be down regulated in parthenocarpic *pro* mutant. As the role of GA in fruit set is downstream from the role of auxin it is still not clear how the developing fruit in *pro* mutant interferes with the expression of *SlHB15A*. One possibility is that GA accumulation in *pro* mutant is interfering with the ovule/integument development where *SlHB15A* is expressed. In line with this, the ovule number was found reduced in both *pro* mutants and in *GA20ox1* over-expression lines (Gomez et al., 2018 and García-Hurtado et al., 2012). On the other hand, in the DAPseq analysis we did not find any direct binding of SlHB15A to key GA biosynthetic or signaling genes, yet we found upregulation of the expression of *GA20ox1*. These data also point toward GA biosynthesis or its signaling cascade, in *pf1* mutant, is the consequence of auxin accumulation and/or ethylene repression (Hu et al., 2018; Serrani et al., 10; Shinozaki et al., 2018).

In summary, our work identified *SlHB15A* as a sentinel to prevent fruit set. In absence of fertilization, *SlHB15A* inhibits auxin biosynthesis and activates biosynthesis of ethylene, maintaining the ovary in a growth-arrest phase. Inactivation of *SlHB15A* or pollination reverses the process, leading to auxin accumulation and repression of ethylene response (Figure 6). As *pf1* mutant accumulates auxin, at anthesis stage; it is likely that the fertilization interferes with the function of *SlHB15A*. It will be of interest to investigate the molecular mechanisms leading to this interference, for example, via identification of repressor of *SlHB15A* function. Our investigation also led to the discovery of *miR166/SlHB15A* regulatory module as a new tool to engineer facultative and obligate parthenocarpy in tomato (Supplemental Text). This could be carried out through the expression of *miRNA166* under cold or heat inducible promoters. Survey of tomato germplasms identified *pat* and *pat-1*, two historical mutants, as alleles of *SlHB15A*. Finally, in addition to the large spectrum of alleles generated in this work, the knowledge generated could also be used as the base to develop plant prototypes producing fruits under adverse conditions.

METHODS

Plant Materials and Growth Conditions

Solanum lycopersicum historical parthenocarpic or seedless mutants were provided by different germplasms distribution centers (See Supplemental Text). The *pf1* mutant was isolated by screening one thousands EMS-mutagenized population derived from *Solanum lycopersicum* cv. M82. Ten thousands plants M2 plants were cultivated to fruit maturity in open field. Blooming and fruit set occurred in June, under an average temperature of ~27 °C (max. 32 °C/ min. 22 °C), affecting significantly the fruiting in M82; harvest and seed counting were performed in August. For experiments within controlled environment, plants were cultivated in pots filled with a mix of peat compost brill (75%): clay (15%): perlite (10%), under a thermoperiod of 25/18 °C (day/night), with 14h light at 4000-6000 Lx and 50-70% relative humidity, as optimal climate. Plants were watered daily and fed every week with 12-12-17 N-P-K fertilizer (Compo, Benelux N.V.). Climate switches were applied progressively over a 4-day period. For heat-stress experiments, plants were grown for 5 weeks under optimal temperature. At the onset of flowering, all pre-existing flowers were removed and the thermoperiod switched to high temperatures. Under 32/26 °C (day/ night), M82/pf1 mutants set no fruits. We then tested 32/24 °C (day/ night), 16/8h (light/dark) photoperiod, 50 – 70% relative humidity. Plants were kept for 4 weeks under these conditions, then 2 weeks under optimal temperatures before harvest. Fruit set was almost completely abolished in wildtype M82 line whereas still effective in the parthenocarpic *pf1* mutant. These conditions, 32/ 24 °C (day/ night) were used for all the heat stress assays. For cold-stress, plants were grown under optimal temperatures for 3 weeks then switched before flowering onset, to 15/12 °C (day/night) temperature, 10/14h (light/dark) photoperiod and 60-70% relative humidity (cold stress conditions), kept for 8 weeks at cold then switched back to optimal temperatures for 3 more days before harvest. Winter field tests were carried out during November to April period. The plants were grown in soil, under insect-proof plastic tunnels with natural light and temperature conditions. No measures were taken to enhance pollination. Average temperature did not exceed 15 ºC for the first two months of the trial, hence below the threshold for pollinated fruit set.

Plant Crosses and Phenotyping

Flowers were emasculated two days before anthesis to prevent self-pollination. For F1 crosses, emasculated flowers were manually pollinated 2 days after emasculation using *pf1/pf1* pollen. WT M82, the Simbad elite or a cherry elite tomato lines were used as female recipient for *pf1/PF1* backrosses and *pf1-3, pf1-6, pat or pat-1* homozygotes for the *pf1/pf1-3, pf1/pf1-6, pf1/pat* and *pf1/pat-1* compound heterozygotes. F1 hybrids were self-pollinated and the phenotype of F2 plants were compared with those of F1 hybrids and their respective parent lines.

For each *pf1* allele, the parthenocarpy was first assessed for more than 10 emasculated flowers per plant, 10 F2 plants per genotype (WT, homozygote, heterozygote or compound heterozygote), cultivated in insect-proof environment. Percentage of developed fruits and seed content were determined at the red-fruit stage. As WT M82 tomato line develops no seedless fruits, the parthenocarpy in *Pf1* M82 can also be scored without emasculation, by counting the seedless fruits produced from plants, vibrated or not. Phenotyping under heat and cold stress conditions was performed on at least 8 plants per genotype and condition. Buzz pollination was applied every day for six weeks from the onset of blooming while no measures were taken to enhance pollination in the “non-vibrated” lots.

Tomato productivity was assessed by harvesting and counting the number of red-ripe and green fruits per plant. The percentage of seedless fruits was assessed on the total amount of ripe fruits for the greenhouse assays. For the field assays, all of the fruits were harvested and weighed to estimate the yields. Individual fruit weight and presence of seeds was evaluated on ~50 fruits per plot. Total soluble solid contents (Brix index) were assessed with a digital refractometer, in juice squeezed from 8 to 12 individual fruits per plant, collected from 6 to 8 parthenocarpic and 6 to 8 non-parthenocarpic sib plants and 4 different sibling replicates.

Ovule phenotype was characterized by light microscopy or scanning-electron microscopy, on anthesis flowers in 3 replicate experiments. The correlation of aberrant ovules and parthenocarpy was asserted at the inflorescence level, by dissecting and phenotyping the ovary of 1 or 2 anthesis flowers and letting the rest of the same inflorescence to develop into parthenocarpic fruits as internal control.

DNA and RNA Preparation

Genomic DNA was extracted from leaf using the DNeasy Plant kit (Qiagen) and total RNAs with the Mirvana Kit (Ambion). RNAs were purified from leaf, total flower at stage 1 to 6 (≤ 1 mm), stage 8 (2 mm), 9 (3 mm), 11 (4 mm), 12 (5 mm), 13 (6 mm), 15 (7 mm) and 16 (8 mm). RNAs were also purified from stage-20 dissected ovaries, ovules, ovules plus placenta, or pericarp and from pollinated flowers at different days after pollination. Shoot-apex RNAs were prepared from M82 or pf1-6/pf1-6 seedlings, cultivated for 18 days under optimal temperature followed by 3 days under cold-stress for the 15-°C samples. The growth being markedly slowed down at cold, the 25-°C-control apices were collected after 1 more day under optimal conditions (hence 19 day-old seedlings) instead of 3 days. Three shoot apices exhibiting several meristematic bulges under stereoscope, hence at the floral-transition stage, were bulked for each sample. Ovules alone or ovules plus placenta were dissected under stereoscope, using razorblades and frozen in liquid nitrogen. Ovule RNAs were prepared from ovules isolated from 10 WT or 15 *pf1* dissected ovaries. The flower-developmental stages were assessed according to (Brukhin et al., 2003).

Bulk Genomic DNA Sequencing and Analysis

Equal amounts of genomic DNA from 10 mutant (P) and 10 non-parthenocarpic (NP) F2 segregants were separately bulked. Genomic DNA libraries were constructed following the standard Illumina protocol. The libraries were sequenced on a HiSeq2000. Sequences were trimmed using Trimmomatic (Bolger et al., 2014) and mapped to the Heinz genome (Tomato Genome Consortium, 2012) (SL3.0) using CLC-Bio (Qiagen), with parameters no_masking, match_score= 1, mismatch_cost= 2, insertion_cost= 3, deletion_cost= 3, length_fraction= 1, similarity_fraction= 0.987. Variants were called initially by retaining high-quality bi-allelic SNPs with >0.1 index, in regions covered at least by 5 reads. Called SNPs were then filtered for EMS-type variants, monomorphic in bulk P as expected for a recessive mutation. A ΔSNP-index, subtracting bulk-P SNP-index by bulk-NP SNP-index (Fekih et al., 2013) was computed, enabling to filter out most variants corresponding to Heinz alleles, sequencing or mapping errors, revealing the causal mutation.

Phylogenetic Analysis

Protein sequences closely homologous to PF1 were isolated from the tomato and *Arabidopsis* genomes, using the Sol Genomics Network (ITAG3.0 release, http://solgenomics.net/) and The Arabidopsis Information Ressource (http://www.arabidopsis.org), by BLAST using a set E-value < $1e^{-10}$. All Arabidopsis and tomato HD-ZipIII proteins were aligned under ClustalW (http://www.ebi.ac.uk/Tools/clustalw). Phylogenetic trees were constructed in MEGA7 (Kumar et al., 2016) (http://www.megasoftware.net/index.html), using the Maximum Likelihood method based on the JTT matrix-based model (Jones et al., 1992). The statistical significance of clades was evaluated with 1000 bootstrap replicates using the same search criteria.

TILLING Screening

PF1 TILLING alleles were isolated from an ethylmethanesulfonate-mutant population of *Solanum lycopersicum* cv M82 described previously (Piron et al., 2010) and from a new generated collection totaling 10,000 M2 families. Both populations were screened by the ENDO1-endonuclease mismatch-detection system as described previously (Piron et al., 2010) or by direct sequencing of target amplicons on a MiSeq system (Illumina) with the primers listed in **Supplemental Table 5**. The putative impact of the Tilling missense alleles on protein function was predicted using the SIFT program (Sim et al., 2012). Induced mutations predicted to impact the function of the protein were backcrossed to the wildtype and the segregation of the mutations with the phenotype was analyzed in F2 plants.

CRISPR/Cas9 Gene Editing

A guide-RNA targeting the *PF1* fifth exon was designed using CRISPR-P (Lei et al., 2014) and joined with the scaffold gRNA and U26 promoter by PCR. Two PCR fragments based on (scafRNA_F, scafRNA_R) and (U26_F, U26_R) primers were amplified from the pCHIMERA plasmid (Leibman-Markus et al., 2018) and combined in a third PCR reaction with (U26_F, scafRNA_R). The resulting product was *AvrII* digested and cloned into the *AvrII* and *StuI* sites of the pMR286 binary vector (Leibman-Markus et al., 2018). *A. tumefaciens* strain *LBA4400, VirG* harboring the pMR286/ *PF1* sgRNA recombinant vector

was used for *S. lycopersicum cv*-M82 transformation as described (Fernandez et al., 2009). Oligonucleotide sequences are listed in **Supplemental Table 5**.

Quantitative Reverse-Transcription PCR

First-strand cDNA synthesis were performed according to the Manufacturer's protocol with Superscript II (Invitrogen) at 43 °C in a 20 µl reaction containing 400 ng total RNAs and dT20VN primer, except for the seedling-apex RNAs reverse transcribed with Superscript IV (Invitrogen) at 51 °C in 20µl with 70 ng total RNA, dT20VN 2.5 µM, miR166a_Rt 0.2 µM and miR166c_Rt 0.2 µM. qPCR were performed with 15-fold diluted cDNAs using MESA-green qPCR mix (Eurogentec) and 0.3 µM of gene-specific primers, on a CFX384 system (Biorad). The expression of HD-ZipIIIs was analyzed by droplet digital PCR, using Evagreen supermix and a QX200 PCR system (Biorad). Actine (Solyc03g078400) was used as reference gene. Oligonucleotide sequences are listed in **Supplemental Table 5**. The qPCR results were analyzed using a ΔΔCt methodology. The flower-developmental stages were assessed according to (Brukhin et al., 2003).

In Situ Hybridization and Histology

In situ hybridizations were performed as described (Nikovics et al., 2006), using a *PF1*-specific riboprobe, a *miR166*-specific LNA probe or a mouse miR LNA probe as negative control. Oligonucleotides are listed in **Supplemental Table 5**. Histology analyses on ovaries, of plants harboring different *PF1* alleles, were carried out on Zeiss LSM880, as described previously (Fonouni-Farde et al., 2019). The flower-developmental stages were assessed according to (Brukhin et al., 2003).

Auxin measurement

Dissected ovaries in three biological replicates were used for measurement of auxin content. For each sample 5mg of dry powder were used. One ng per sample of Indole-3-acetic acid stable labelled isotopes were used as internal standards as described in Le Roux et al. (2014). Auxin extractions and measurements were carried out as described in Ligerot et al. (2017).

Ethylene measurement

Dissected ovaries in three biological replicates were used for measurement of ethylene production. Ovaries at each stage were dissected, weighed and enclosed in a 10–mL glass chromatography vial incubated under darkness at 25°C for 2 hours. The vials were flushed with hydrocarbon free air (Air Liquide) at a flow rate of 3 L.h−1 and ethylene in the headspace was measured with an ETD-300 photo-acoustic detector (Sensor Sense B.V., Nijmegen, Netherlands).

DAPseq Analysis

For DAPseq, the *PF1* CDS was isolated from flower RNA, by RT-PCR with (Tom277, Tom278) and joined to Gateway-cloning sites by PCR with (Tom029, Tom030) primers. The resulting product was cloned into pDONOR222 and transferred into pIX-HALO by Gateway recombination according to the Manufacturer's protocol (Invitrogen). Expression of Halo-PF1 fusion and enrichment of DNA targets were performed as described previously (O'Malley et al. 2016). DNA library preparations were performed following the manufacturer's protocol (Illumina) and sequenced on a NextSeq500 as 2x 75 nt reads.

Electrophoretic Mobility Shift Assay

The full-length coding sequence of SlHB15A was cloned into the GST fusion vector pDEST15 and introduced into *Escherichia coli* strain BL21 Rosetta. The GST::SlHB15A recombinant protein or GST-tag alone were induced in a 500 mL expression culture using 0.4 mM IPTG (Isopropyl β-D-1-thiogalactopyranoside), and cells were harvested 16 h after induction at 18ºC. Cells were lysed using a combination of lysozyme treatment and sonication. Supernatant of the centrifuged lysate was used for GST-tag affinity purification using 0.5 mL Protino Glutathione Agarose 4B medium (Macherey-Nagel). Eluates were analyzed by SDS-PAGE and Coomassie Brilliant Blue staining. Protein concentration was determined by the Bradford assay (Bradford, 1976). Probes harboring cis-elements were synthesized and labeled with biotin at their 5′ end. For probe competition, unlabeled probe was added to the reactions. EMSA was performed using the lightshift chemiluminescent EMSA kit (Thermo Fisher Scientific, USA) with 7 µg of recombinant protein per binding reaction. Probe sequences are listed in Supplemental Table 5.

RNAseq Analysis

Flower and ovules RNAseq libraries were constructed according to Illumina instructions and sequenced on Hiseq 4000 platform at Novogene Co. Ltd. Raw sequencing reads were cleaned by removing adaptor sequences and low-quality reads. The resulting high-quality reads were mapped to the tomato genome (Tomato Genome Consortium, 2012) (ITAG3.2) using STAR, with default parameters. Gene expression was quantified using featureCounts with default parameters (Liao et al., 2014). Read count normalization and differential expression analysis were performed using DESeq2 (Love et al., 2014). Differentially expressed genes in *pf1* ovules as compared to wildtype, with adjusted *P*-value ≤0.01 and ratio ≥2 or ratio ≤0.5 were filtered for subsequent analyses.

For the fertilized and un-fertilized wildtype M82 ovules collected at 1, 2 or 5 days post anthesis, RNAseq data were retrieved from the NCBI's Gene Expression Omnibus, accession number GSE72216 (Zhang et al., 2016). Bioinformatic analysis of GSE72216 data were done as described above.

Gene-list comparison and Venn diagrams were performed online at http://bioinformatics.psb.ugent.be/webtools/Venn. The statistical significance of the overlaps was calculated using the hypergeometric test (http://nemates.org/MA/progs/overlap_stats.html). Analysis of gene-ontology terms enrichment was performed using ShyniGO (Ge et al., 2020).

Statistical Analyses

All experiments were carried out in at least 3 replicates. The fruit-set phenotype was analyzed in randomized block design experiments. Student's t test, Tukey's test and hypergeometric test were used to assess the statistical significance of the results, as described in the above corresponding section of the Material and Methods, the Supplemental Text and the figure legends.

ACCESSION NUMBERS

Raw sequence data from this study have been deposited in the NCBI Short Read Archive database under the following accession numbers: SAMN16792678, SAMN16792679 (bulked-genome sequence from *pf1* parthenocarpic and non-parthenocarpic plants); SAMN16792680 to -85 (DAPseq); SAMN16792686, SAMN16792687, SAMN16816096 to -99 and

SAMN18442419 to -23 (RNAseq). All de-novo *pf1* mutant alleles from this study are available with standard MTA upon request

FUNDING

The work was supported by INRAE, CNRS, and the LabEx Saclay Plant Sciences - SPS (ANR-10-LABX-40-SPS). AB team received funding the European Research Council (ERC-SEXYPARTH, 341076) and from Horizon 2020 research and innovation programme (TOMRES, 727929).

AUTHOR CONTRIBUTIONS

C.C. conceived, conducted, analyzed the experiments and interpreted the results. C.C., JC.L., S.K. and Y.H. contributed to genetic and phenotypic characterization of the mutants. C.C., A.Bo. and A.Be. contributed to bulk-genome sequence analysis. F.M. and C.C. contributed to TILLING screen. H.M., C.C. and Y.H contributed to histology, scanning-electron microscopy and in-situ hybridizations which were analyzed by C.C.; C.C. and Y.H. performed qPCR expression studies; A.Bo., C.C., B.M. and M.V. contributed to RNAseq. R.B. and R.S.D. performed CRISPR and DAPseq experiments. A.Bo. M.V and C.C. analyzed the DAPseq data. C.C. and R.S.D. contributed to EMSA analysis. C.C., S.C. and G.M. contributed to auxin analysis. C.C. and G.B. contributed to ethylene analysis. A.Be. conceived and supervised the study. C.C. and A.Bo prepared the figures. C.C. and A.Be wrote the manuscript with contribution from A.Bo. All authors read and approved the final manuscript.

ACKNOWLEDGMENTS

We thank Martin Crespi and Reiner Veitia for fruitful discussions, Judit Szecsi and Youssef Belkhadir for careful proofreading of the manuscript; Afef Lemhamdi, Julien Brunel, Pascal Audigier and Holger Ornstrup for technical assistance.

COMPETING INTERESTS

The authors declare no competing interests.

REFERENCES

Abdul-Baki, A.A., and Stommel, J.R. (1995). Pollen Viability and Fruit Set of Tomato Genotypes under Optimumand High-temperature Regimes. HortScience HortSci 30, 115.

Bolger, A.M., Lohse, M., and Usadel, B. (2014). Trimmomatic: a flexible trimmer for Illumina sequence data. Bioinformatics 30:2114-2120.

Bradford, M.M. (1976). A rapid and sensitive method for the quantita- tion of microgram quantities of protein utilizing the principle of protein- dye binding. Anal. Biochem. 72: 248–254.

Brandt, R., Salla-Martret, M., Bou-Torrent, J., Musielak, T., Stahl, M., Lanz, C., Ott, F., Schmid, M., Greb, T., Schwarz, M., et al. (2012). Genome-wide binding-site analysis of REVOLUTA reveals a link between leaf patterning and light-mediated growth responses. Plant J 72:31-42.

Brukhin, V., Hernould, M., Gonzalez, N., Chevalier, C., and Mouras, A. (2003). Flower development schedule in tomato Lycopersicon esculentum cv. sweet cherry. Sexual Plant Reproduction 15:311-320.

Carbonell-Bejerano, P., Urbez, C., Granell, A., Carbonell, J. & Perez-Amador, M.A. (2011). Ethylene is involved in pistil fate by modulating the onset of ovule senescence and the GA-mediated fruit set in Arabidopsis. *BMC Plant Biol* **11**, 84

Charles, W.B., and Harris, R.E. (1972). Tomato Fruit-Set at High and Low Temperatures. Can J Plant Sci 52:497-506.

Cooper, D.C. (1931). Macrosporogenesis and the development of the macrogametophyte of lycopersicon Esculentum. Am J Bot 18:739-748.

da Silva, E.M., Silva, G.F.F.E., Brussolo Bidoia, D., da Silva Azevedo, M., Almeida de Jesus, F., Pino, L.E., Peres, L.E.P., Carrera, E., Lopez-Diaz, I., and Nogueira, F.T.S. (2017). microRNA159-targeted SlGAMYB transcription factors are required for fruit set in tomato. Plant J 92:95-109.

de Jong, M., Mariani, C., and Vriezen, W.H. (2009a). The role of auxin and gibberellin in tomato fruit set. J Exp Bot 60:1523-1532.

de Jong, M., Wolters-Arts, M., Feron, R., Mariani, C., and Vriezen, W.H. (2009b). The Solanum lycopersicum auxin response factor 7 (SlARF7) regulates auxin signaling during tomato fruit set and development. Plant J 57:160-170.

Deutschbauer, A.M., Jaramillo, D.F., Proctor, M., Kumm, J., Hillenmeyer, M.E., Davis, R.W., Nislow, C., and Giaever, G. (2005). Mechanisms of haploinsufficiency revealed by genome-wide profiling in yeast. Genetics 169:1915-1925.

Dorcey, E., Urbez, C., Blázquez, M.A., Carbonell, J. & Perez-Amador, M.A. (2009). Fertilization-dependent auxin response in ovules triggers fruit development through the modulation of gibberellin metabolism in Arabidopsis. *Plant J* **58**, 318-332

Erickson, A.N., and Markhart, A.H. (2002). Flower developmental stage and organ sensitivity of bell pepper (Capsicum annuum L.) to elevated temperature. Plant Cell and Environment 25, 123-130.

Fekih, R., Takagi, H., Tamiru, M., Abe, A., Natsume, S., Yaegashi, H., Sharma, S., Sharma, S., Kanzaki, H., Matsumura, H., et al. (2013). MutMap+: genetic mapping and mutant identification without crossing in rice. PloS one 8:e68529.

Fernandez, A.I., Viron, N., Alhagdow, M., Karimi, M., Jones, M., Amsellem, Z., Sicard, A., Czerednik, A., Angenent, G., Grierson, D., et al. (2009). Flexible tools for gene expression and silencing in tomato. Plant Physiol 151:1729-1740.

Firon, N., Shaked, R., Peet, M.M., Pharr, D.M., Zamski, E., Rosenfeld, K., Althan, L., and Pressman, E. (2006). Pollen grains of heat tolerant tomato cultivars retain higher carbohydrate concentration under heat stress conditions. Scientia Horticulturae 109, 212-217.

Fonouni-Farde, C., Miassod, A., Laffont, C., Morin, H., Bendahmane, A., Diet, A., and Frugier, F. (2019). Gibberellins negatively regulate the development of Medicago truncatula root system. Sci Rep 9:2335.

Garcia-Hurtado, N., Carrera, E., Ruiz-Rivero, O., López-Gresa, M. P., Hedden, P., Gong, F., García-Martínez J. L. (2012).The characterization of transgenic tomato overexpressing gibberellin 20-oxidase reveals induction of parthenocarpic fruit growth, higher yield, and alteration of the gibberellin biosynthetic pathway. *J Exp Bot* **63**, 5803-5813.

Ge, S.X., Jung, D., and Yao, R. (2020). ShinyGO: a graphical gene-set enrichment tool for animals and plants. Bioinformatics 36:2628-2629.

Giorno, F., Wolters-Arts, M., Mariani, C., and Rieu, I. (2013). Ensuring Reproduction at High Temperatures: The Heat Stress Response during Anther and Pollen Development. Plants (Basel) 2, 489-506.

Gomez, M.D., Ventimilla, D., Sacristan, R., and Perez-Amador, M.A. (2016). Gibberellins Regulate Ovule Integument Development by Interfering with the Transcription Factor ATS. Plant Physiol 172:2403-2415.

Gomez MD, Barro-Trastoy D, Escoms E, Saura-Sánchez M, Sánchez I, Briones-Moreno et al.. (2018). Gibberellins negatively modulate ovule number in plants. Development. 145:163865.

Gorguet, B., Eggink, P.M., Ocana, J., Tiwari, A., Schipper, D., Finkers, R., Visser, R.G., and van Heusden, A.W. (2008). Mapping and characterization of novel parthenocarpy QTLs in tomato. Theor Appl Genet 116:755-767.

Hao, S., Ariizumi, T., and Ezura, H. (2017). SEXUAL STERILITY is Essential for Both Male and Female Gametogenesis in Tomato. Plant Cell Physiol 58:22-34.

Hashimoto, K., Miyashima, S., Sato-Nara, K., Yamada, T., and Nakajima, K. (2018). Functionally Diversified Members of the MIR165/6 Gene Family Regulate Ovule Morphogenesis in Arabidopsis thaliana. Plant Cell Physiol 59:1017-1026.

Hu, J., Israeli, A., Ori, N. and Sun, T. P. (2018). The interaction between DELLA and ARF/IAA mediates crosstalk between gibberellin and auxin signaling to control fruit initiation in tomato. Plant Cell 30, 1710–1728

Johnson, A.F., Nguyen, H.T., and Veitia, R.A. (2019). Causes and effects of haploinsufficiency. Biol Rev Camb Philos Soc 94:1774-1785.

Joldersma, D., and Liu, Z. (2018). The making of virgin fruit: the molecular and genetic basis of parthenocarpy. J Exp Bot 69:955-962.

Jones, D.T., Taylor, W.R., and Thornton, J.M. (1992). The rapid generation of mutation data matrices from protein sequences. Comput Appl Biosci 8:275-282.

Jones-Rhoades, M.W., Bartel, D.P. and Bartel, B. (2006) MicroRNAs and their regulatory roles in plants. Ann. Rev. Plant Biol. 57, 19–53.

Kelley, D.R., Skinner, D.J., and Gasser, C.S. (2009). Roles of polarity determinants in ovule development. Plant J 57:1054-1064.

Kim, J., Jung, J.H., Reyes, J.L., Kim, Y.S., Kim, S.Y., Chung, K.S., Kim, J.A., Lee, M., Lee, Y., Narry Kim, V., et al. (2005). microRNA-directed cleavage of ATHB15 mRNA regulates vascular development in Arabidopsis inflorescence stems. Plant J 42:84-94.

Kumar, S., Stecher, G., and Tamura, K. (2016). MEGA7: Molecular Evolutionary Genetics Analysis Version 7.0 for Bigger Datasets. Mol Biol Evol 33:1870-1874.

Le Roux C, Del Prete S, Boutet-Mercey S, Perreau F, Balagué C, Roby D, Fagard M, Gaudin V. (2014) The hnRNP-Q protein LIF2 participates in the plant immune response. PLoS One. 2014; 9(6):e99343.

Lei, Y., Lu, L., Liu, H.Y., Li, S., Xing, F., and Chen, L.L. (2014). CRISPR-P: a web tool for synthetic single-guide RNA design of CRISPR-system in plants. Mol Plant 7:1494-1496.

Leibman-Markus, M., Pizarro, L., Schuster, S., Lin, Z.J.D., Gershony, O., Bar, M., Coaker, G., and Avni, A. (2018). The intracellular nucleotide-binding leucine-rich repeat receptor (SlNRC4a) enhances immune signaling elicited by extracellular perception. Plant, cell & environment 41:2313-2327.

Liao, Y., Smyth, G.K., and Shi, W. (2014). featureCounts: an efficient general purpose program for assigning sequence reads to genomic features. Bioinformatics 30:923-930.

Liu, N., Wu, S., Van Houten, J., Wang, Y., Ding, B., Fei, Z., Clarke, T.H., Reed, J.W. and Esther van der Knaap, E. (2014) Down-regulation of AUXIN RESPONSE FACTORS 6 and 8 by microRNA 167 leads to floral development defects and female sterility in tomato. J. Exp. Bot. 65, 2507–2520.

Ligerot, Y., de Saint Germain, A., Waldie, T., Troadec, C., Citerne, S., Kadakia, N., Pillot, J.P., Prigge, M., Aubert, G., Bendahmane, A., et al. (2017) The pea branching RMS2 gene encodes the PsAFB4/5 auxin receptor and is involved in an auxin-strigolactone regulation loop. PLoS Genet. 8;13:e1007089

Lin, T., Zhu, G., Zhang, J., Xu, X., Yu, Q., Zheng, Z., Zhang, Z., Lun, Y., Li, S., Wang, X., et al. (2014). Genomic analyses provide insights into the history of tomato breeding. Nat Genet 46:1220-1226.

Lopez-Gomollon, S., Mohorianu, I., Szittya, G., Moulton, V., and Dalmay, T. (2012). Diverse correlation patterns between microRNAs and their targets during tomato fruit development indicates different modes of microRNA actions. Planta 236:1875-1887.

Love, M.I., Huber, W., and Anders, S. (2014). Moderated estimation of fold change and dispersion for RNA-seq data with DESeq2. Genome Biol 15:550.

Marti, C., Orzáez, D., Ellul, P., Moreno, V., Carbonell, J., Granell A. (2007). Silencing of DELLA induces facultative parthenocarpy in tomato fruits. *Plant J* **52**, 865-876.

Mazzucato, A., Taddei, A.R., and Soressi, G.P. (1998). The parthenocarpic fruit (*pat*) mutant of tomato (Lycopersicon esculentum Mill.) sets seedless fruits and has aberrant anther and ovule development. Development 125:107-114.

Nikovics, K., Blein, T., Peaucelle, A., Ishida, T., Morin, H., Aida, M., and Laufs, P. (2006). The balance between the MIR164A and CUC2 genes controls leaf margin serration in Arabidopsis. Plant Cell 18:2929-2945.

Okabe Y, Yamaoka T, Ariizumi T, Ushijima K, Kojima M, Takebayashi Y, Sakakibara H, et al. (2019) Aberrant Stamen Development is Associated with Parthenocarpic Fruit Set Through Up-Regulation of Gibberellin Biosynthesis in Tomato. Plant Cell Physiol. 60:38-51.

O'Malley, R.C., Huang, S.C., Song, L., Lewsey, M.G., Bartlett, A., Nery, J.R., Galli, M., Gallavotti, A., and Ecker, J.R. (2016). Cistrome and Epicistrome Features Shape the Regulatory DNA Landscape. Cell 166:1598.

Omidvar, V., Mohorianu, I., Dalmay, T., and Fellner, M. (2015). MicroRNA Regulation of Abiotic Stress Response in 7B-1 Male-Sterile Tomato Mutant. Plant Genome-Us 8:plantgenome2015.2002.0008.

Pattison, R.J. , Csukasi, F., Zheng, Y., Fei, Z., van der Knaap, E., Catalá, C. (2015). Comprehensive Tissue-Specific Transcriptome Analysis Reveals Distinct Regulatory Programs during Early Tomato Fruit Development. *Plant Physiol* **168**, 1684-1701.

Pecaut, J., and Philouze, J. (1978). A *sha*/*pat* line obtained by natural mutation. Rep. Tom. Genet. Coop. 28:12.

Peet, M.M., Sato, S., and Gardner, R.G. (1998). Comparing heat stress effects on male-fertile and male-sterile tomatoes. Plant Cell and Environment 21:225-231.

Philouze, J., and Maisonneuve, B. (1978a). Heredity of the natural ability to set parthenocarpic fruits in a German line. Tomato Genetics Cooperative Report 28:12.

Philouze, J., and Maisonneuve, B. (1978b). Heredity of the natural ability to set parthenocarpic fruits in the Soviet variety Severianin. Tomato Genetics Cooperative Report 28:12-13.

Pillitteri, L.J., Bemis, S.M., Shpak, E.D., and Torii, K.U. (2007). Haploinsufficiency after successive loss of signaling reveals a role for ERECTA-family genes in Arabidopsis ovule development. Development 134:3099-3109.

Piron, F., Nicolai, M., Minoia, S., Piednoir, E., Moretti, A., Salgues, A., Zamir, D., Caranta, C., and Bendahmane, A. (2010). An induced mutation in tomato eIF4E leads to immunity to two potyviruses. PloS one 5:e11313.

Pnueli, L., Carmel-Goren, L., Hareven, D., Gutfinger, T., Alvarez, J., Ganal, M., Zamir, D., and Lifschitz, E. (1998). The SELF-PRUNING gene of tomato regulates vegetative to reproductive switching of sympodial meristems and is the ortholog of CEN and TFL1. Development 125:1979-1989.

Rodriguez, G.R., Munos, S., Anderson, C., Sim, S.C., Michel, A., Causse, M., Gardener, B.B., Francis, D., and van der Knaap, E. (2011). Distribution of SUN, OVATE, LC, and FAS in the tomato germplasm and the relationship to fruit shape diversity. Plant Physiol 156:275-285.

Rotino, G.L., Perri, E., Zottini, M., Sommer, H., and Spena, A. (1997). Genetic engineering of parthenocarpic plants. Nat Biotechnol 15:1398-1401.

Sato, S., Peet, M.M., and Thomas, J.F. (2000). Physiological factors limit fruit set of tomato (Lycopersicon esculentum Mill.) under chronic, mild heat stress. Plant Cell and Environment 23, 719-726.

Serrani, J.C., Sanjuan, R., Ruiz-Rivero, O., Fos, M., and Garcia-Martinez, J.L. (2007). Gibberellin regulation of fruit set and growth in tomato. Plant Physiol 145:246-257.

Serrani, J.C., Ruiz-Rivero, O., Fos, M. & Garcia-Martinez, J.L. (2008).Auxin-induced fruit-set in tomato is mediated in part by gibberellins. *Plant J* **56**, 922-934

Sessa, G., Carabelli, M., Possenti, M., Morelli, G., and Ruberti, I. (2018). Multiple Links between HD-Zip Proteins and Hormone Networks. Int J Mol Sci 19.

Shinozaki, Y., Ezura, H., and Ariizumi, T. (2018). The role of ethylene in the regulation of ovary senescence and fruit set in tomato (Solanum lycopersicum). Plant Signal Behav 13:e1146844.

Shinozaki, Y., Beauvoit, P.B., Takahara, M., Hao, S., Ezura, K., et al. (2020). Fruit setting rewires central metabolism via gibberellin cascades. Proc Natl Acad Sci U S A 117:23970-23981

Sim, N.L., Kumar, P., Hu, J., Henikoff, S., Schneider, G., and Ng, P.C. (2012). SIFT web server: predicting effects of amino acid substitutions on proteins. Nucleic Acids Res 40:W452-457.

Skinner, D.J., Brown, R.H., Kuzoff, R.K., and Gasser, C.S. (2016). Conservation of the role of INNER NO OUTER in development of unitegmic ovules of the Solanaceae despite a divergence in protein function. BMC Plant Biol 16:143.

Soressi, G.P., and Salamini, F. (1975). A monomendellian gene inducing parthenocarpic fruits. Rep. Tom. Genet. Coop. 25:22.

Tomato Genome Consortium (2012). The tomato genome sequence provides insights into fleshy fruit evolution. Nature 485:635-641.

Wang, H., Liu, Y., Bruffett, K., Lee, J., Hause, G., Walker, J.C., and Zhang, S. (2008). Haplo-insufficiency of MPK3 in MPK6 mutant background uncovers a novel function of these two MAPKs in Arabidopsis ovule development. Plant Cell 20:602-613.

Wang, H., Schauer, N., Usadel, B., Frasse, P., Zouine, M., Hernould, M., Latche, A., Pech, J.C., Fernie, A.R., and Bouzayen, M. (2009). Regulatory features underlying pollination-dependent and -independent tomato fruit set revealed by transcript and primary metabolite profiling. Plant Cell 21:1428-1452.

Wang, R., Angenent, G.C., Seymour, G., and de Maagd, R.A. (2020). Revisiting the Role of Master Regulators in Tomato Ripening. Trends in plant science 25:291-301.

Wilkie JD, Sedgley M and Olesen T. (2008) Regulation of floral initiation in horticultural trees. J Exp Bot. 59:3215-28.

Qian Xu, Rong Li, Lin Weng, Yuan Sun, Meng Li, Han Xiao. (2019). Domain-specific expression of meristematic genes is defined by the LITTLE ZIPPER protein DTM in tomato Commun Biol. 2019; 2: 134.

Xu, S., and Chong, K. (2018). Remembering winter through vernalisation. Nat Plants 4:997-1009.

Zhang, S., Xu, M., Qiu, Z., Wang, K., Du, Y., Gu, L., and Cui, X. (2016). Spatiotemporal transcriptome provides insights into early fruit development of tomato (Solanum lycopersicum). Sci Rep 6:23173.

Zhang, T., Li, Y., Ma, L., Sang, X., Ling, Y., Wang, Y., Yu, P., Zhuang, H., Huang, J., Wang, N., et al. (2017). LATERAL FLORET 1 induced the three-florets spikelet in rice. Proc Natl Acad Sci U S A 114:9984-9989.

Zhao, C., Liu, B., Piao, S., Wang, X., Lobell, D.B., Huang, Y., Huang, M., Yao, Y., Bassu, S., Ciais, P., et al. (2017a). Temperature increase reduces global yields of major crops in four independent estimates. Proc Natl Acad Sci U S A 114:9326-9331.

Zhao, X., Bramsiepe, J., Van Durme, M., Komaki, S., Prusicki, M.A., Maruyama, D., Forner, J., Medzihradszky, A., Wijnker, E., Harashima, H., et al. (2017b). RETINOBLASTOMA RELATED1 mediates germline entry in Arabidopsis. Science 356:eaaf6532.

Zinn, K.E., Tunc-Ozdemir, M., and Harper, J.F. (2010). Temperature stress and plant sexual reproduction: uncovering the weakest links. J Exp Bot 61:1959-1968.

FIGURE LEGENDS

Figure 1. *pf1* confers obligate parthenocarpy under adverse heat conditions.

Developing and mature fruits from wildtype fertilized flowers (A, B) and *pf1/pf1* unfertilized flowers (C, D). Parthenocarpic fruit is seedless (D) and develops on top of the corolla (C). Introgression of *pf1* allele in fresh-market (E, F) and cherry (G, H) tomatoes leads to parthenocarpic fruit set (F, H). E and G: *PF1/PF1* wildtype pollinated fruits. A to H: plants grown at 25°C. Fruit set of pollinated (Vi) and unpollinated (NV) tomato genotypes grown at 25 °C (I-K) or 32 °C (L-N). Leaves were removed to show the fruits. (O) Number of developed fruits per plant. (P) Percentage of seedless fruits at harvest for each genotype grown at 25 °C or 32 °C. Values are means ±S.D. derived from 5 plants. Two-tailed unpaired Student's *t*-test was used to determine the significance of the indicated comparisons. Significance levels: $**P < 0.01$. n.s: no statistically significant difference. (Q) Distribution of Δ(SNP-index) long chromosome 3, calculated with a 1-Mb-sliding window. The highest genome-wide Δ(SNP-index) (red triangle) corresponds to a G-to-A nonsense mutation in gene *Solyc03g120910*. (R) Structure of *PF1/SlHB15A* gene and induced alleles leading to obligate parthenocarpy. UTRs and coding sequence are indicated as hollow and filled boxes, respectively. Scale bars represent 1cm in A to D; 2 cm in E to H; 10 cm in I to N.

Figure 2. *pf1* alleles confer conditional parthenocarpy at cold.

(A-I) Fruit set of tomato genotypes grown at 25°C (A-C, J-L) or 15°C (D-F, M-O). In *pf1/pf1* plants, parthenocarpic fruits develop at any conditions (C, F). Conditional parthenocarpy occurs in *pf1* heterozygous plants only at 15°C (E), yielding fruits similar in size (G, H right) to pollinated fruits (left). (J-Q) *pf1-3* hypomorphic allele, not parthenocarpic under optimal temperature (J-L), expresses conditional parthenocarpy at 15°C (N, O). Number of ripe fruits per plant (I, P) and percentage of seedless fruits (Q) at harvest for each genotype and stress condition. Vi, pollinated. NV, unpollinated. Values are means ±S.D. derived from at least 6 plants. Two-tailed Student's *t*-test was used to determine the significance of the indicated comparisons. Significance levels: $*P < 0.05$, $**P < 0.01$, $***P < 0.001$. n.s: no statistically significant difference. Plants were defoliated to show the fruits. Scale bars represent 10 cm in A to O; 2 cm in G and H.

Figure 3. Cold-induced *miR166* controls *SlHB15A*-mediated parthenocarpy.

(A) Expression analysis of *PF1* in leaf, shoot apex and stage-1-to-11 flowers (St1-11). Values are means ±S.D. derived from 3 plants. (B) *miR166*-base pairing with *PF1* and *miR166*-resistant *pf1-6* transcripts. (C, D, K-P) *In-situ* hybridizations of *miR166* (C, D) and *PF1* (K-P) in shoot apex and flower. (O) Stage-16 ovary; (P) Ovule magnification; IM, FM, TM ,SYM and SAM indicate inflorescence, flower, transition, sympodial and shoot apical meristems, respectively; S1, stage-1-flower-meristem dome; V, vascular elements; In, integument-outer-cell layer; CW, carpel wall; Ov, ovule; Pl, placenta; L, leaf; S, sepal. bars= 100 µm. Arrowheads highlight PF1 expression. (E-J) Fruit set of unpollinated (NV) tomato genotypes at 25°C (E, G, I) or 15°C (F, H, J). Leaves were removed to show the fruits. bars= 10 cm (Q) qPCR analysis of *miR166* transcripts in 3-week-old apices of *PF1/PF1* and *pf1-6/pf1-6* plants grown at 15°C or 25°C. Values are means ±S.D. derived from 3 plants. (R) Relative abundance assessed by RNAseq of wildtype *PF1 versus miR166*-resistant *pf1-6* transcripts in *PF1/pf1-6* heterozygotes grown at 25°C or 15°C. Values are means ±S.D. of *PF1 and pf1-6* reads spanning the *pf1-6* mutation locus derived from 3 RNAseq experiments. RE: relative expression. (S) Number of seedless fruits per plant. Values are means ±S.D. derived from 9 plants. Two-tailed Student's *t*-test was used to determine the significance of the indicated comparisons. Significance levels: $*P < 0.05$, $**P < 0.01$, $***P < 0.001$. n.s: no statistically significant difference.

Figure 4. A gradient of aberrant ovules correlates with parthenocarpy in *pf1* plants.

Confocal images of stage-18 wildtype-anatropous (**A**) and *pf1*-aberrant ovule showing no integument (In) and uncovered nucellus (Nu) (B). (**C**) Scanning-electron micrograph of anthesis normal-looking (Ov) and aberrant (Ab) ovules in *pf1/pf1*. (**D-I**) Light micrographs of dissected ovaries developed under optimal (25 °C) or cold (15 °C) conditions. Asterisks highlight aberrant ovules in (H), arrowheads normal ovules in (F and I). (J) Parthenocarpy and ovule phenotypes of various *pf1*-allele combinations under optimal and cold conditions. Mean percentages ±S.D. were averaged from at least 3 series of 2 ovaries. Different letters represent statistically significant differences within each temperature condition, according to one-way ANOVA with Tukey's post hoc test ($P < 0.01$). Scale bars= 100 µm (A to C) 500 µm (D to I).

Figure 5. *pf1*-aberrant ovules mimic fertilized ovules.

(A) Shared DEGs between *pf1*-aberrant *vs* wildtype-unfertilized ovules and wildtype-unfertilized *vs* -pollinated ovules at 1, 2 and 5 days post pollination (DPP). (**B**) GO analysis of the upregulated (orange) and downregulated (blue) genes. (**C**) Analysis of PF1-enriched regions in the DAPseq assay. Pie chart showing the percentage distribution of PF1-binding peaks in each category. (**D**) PF1 DNA-binding motif. (**E**) Overlap between the up- and downregulated genes in *pf1*-aberrant ovules and PF1-bound genes. Hypergeometric test *P*-values are indicated. (**F**) Genome browser view of the distribution of the DAPseq reads (grey, HALO control; orange, PF1) of auxin and ethylene genes and their corresponding relative expression (RE) in aberrant ovules (*pf1*) and wildtype ovules at anthesis (A) or at 5 DPP (P). (**G**) EMSAs showing that SlHB15A binds to the *ToFZY2* and *SlERF.F1* cis regulatory elements. Competition for binding was performed using 20 pmol and 90 pmol of unlabeled probes. GST was used as negative control. (H,I) IAA content (H) and ethylene production (I) in wildtype *PF1* fertilized (P) and unfertilized (UP) ovaries and *pf1* unfertilized (UP) ovaries at 0, 2 and 4 days after anthesis (DAA), ND: not detected. Two-tailed Student's *t*-test was used to determine the significance of the indicated comparisons. Significance levels: $*P < 0.05$, $**P < 0.01$, $***P < 0.001$. n.s: no statistically significant difference. DW: dry weight. FW: fresh weight.

Figure 6. Working model explaining how *miR166-SlHB15* regulatory module controls ovule development and fruit set.

(A) In the absence of fertilization, PF1 inhibits auxin- and activates ethylene signaling, maintaining the ovary in a growth-arrest phase until pollination takes place. (B) Ovule fertilization relieves the inhibition; accumulation of auxin and inhibition of ethylene signaling lead to fruit set. (C) *pf1* loss of function alleles induce aberrant ovules that mimic wildtype pollinated ovules. (D) In *Pf1/pf1* heterozygote plants, under cold conditions, the overexpression of *miR166* knockdowns *PF1* mRNA to threshold leading to aberrant ovules and fruit set.

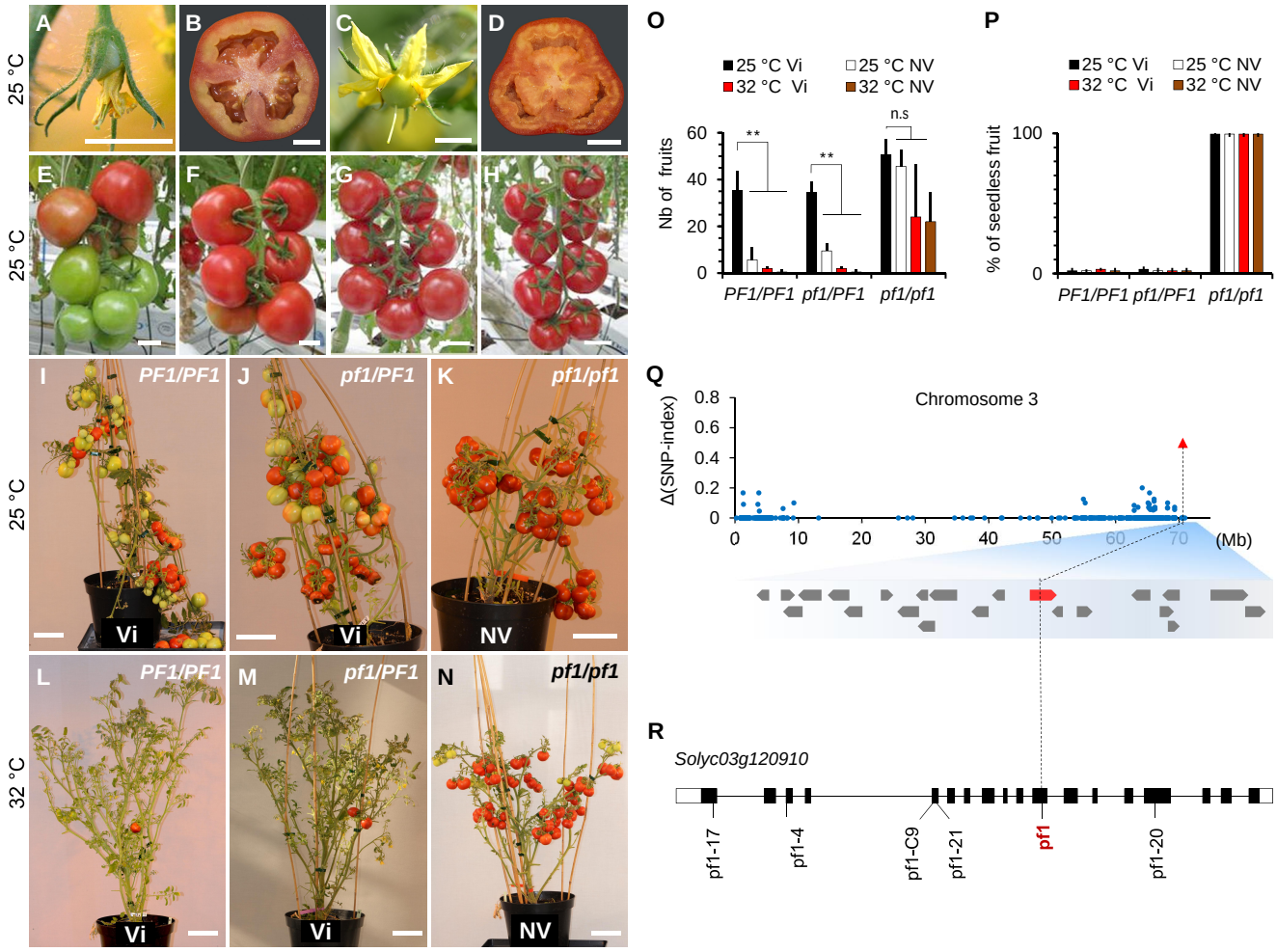
25 °C
25 °C
25 °C
32 °C
A
B
C
D
E
F
G
H
I
PF1/PF1
J
pf1/PF1
K
pf1/pf1
Vi
Vi
NV
L
PF1/PF1
M
pf1/PF1
N
pf1/pf1
Vi
Vi
NV
O
25 °C Vi
25 °C NV
32 °C Vi
32 °C NV
Nb of fruits
60
40
20
0
**
**
n.s
PF1/PF1
pf1/PF1
pf1/pf1
P
25 °C Vi
25 °C NV
32 °C Vi
32 °C NV
% of seedless fruit
100
0
PF1/PF1
pf1/PF1
pf1/pf1
Q
Chromosome 3
Δ(SNP-index)
0.8
0.6
0.4
0.2
0
0
10
20
30
40
50
60
70
(Mb)
R
Solyc03g120910
pf1-17
pf1-4
pf1-C9
pf1-21
pf1
pf1-20

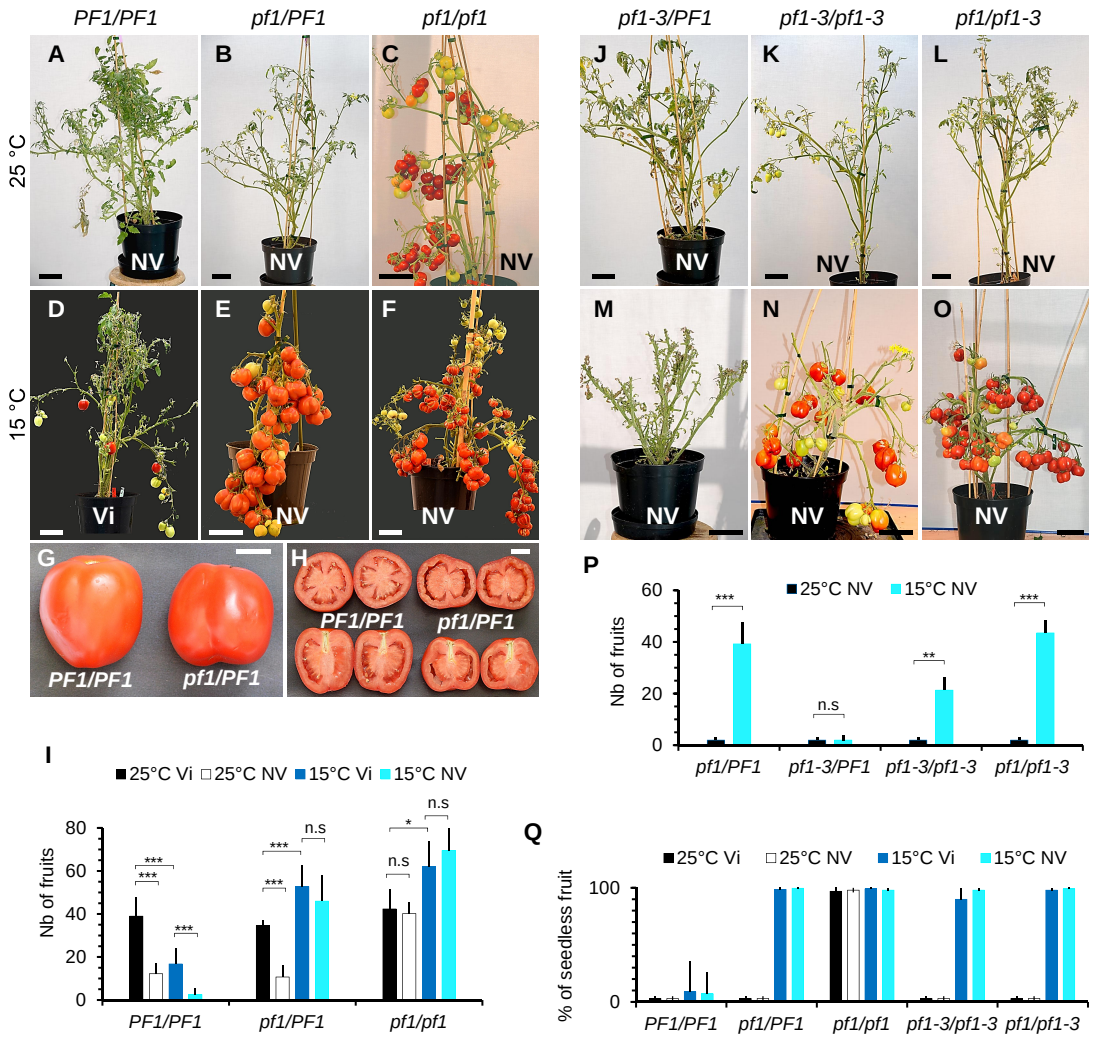
PF1/PF1
pf1/PF1
pf1/pf1
pf1-3/PF1
pf1-3/pf1-3
pf1/pf1-3
25 °C
15 °C
A
B
C
J
K
L
D
E
F
M
N
O
NV
Vi
G
H
PF1/PF1
pf1/PF1
P
25°C NV
15°C NV
Nb of fruits
60
40
20
0
***
n.s
**
pf1/PF1
pf1-3/PF1
pf1-3/pf1-3
pf1/pf1-3
I
25°C Vi
25°C NV
15°C Vi
15°C NV
Nb of fruits
80
60
40
20
0
n.s
*
PF1/PF1
pf1/PF1
pf1/pf1
Q
25°C Vi
25°C NV
15°C Vi
15°C NV
% of seedless fruit
100
0
PF1/PF1
pf1/PF1
pf1/pf1
pf1-3/pf1-3
pf1/pf1-3

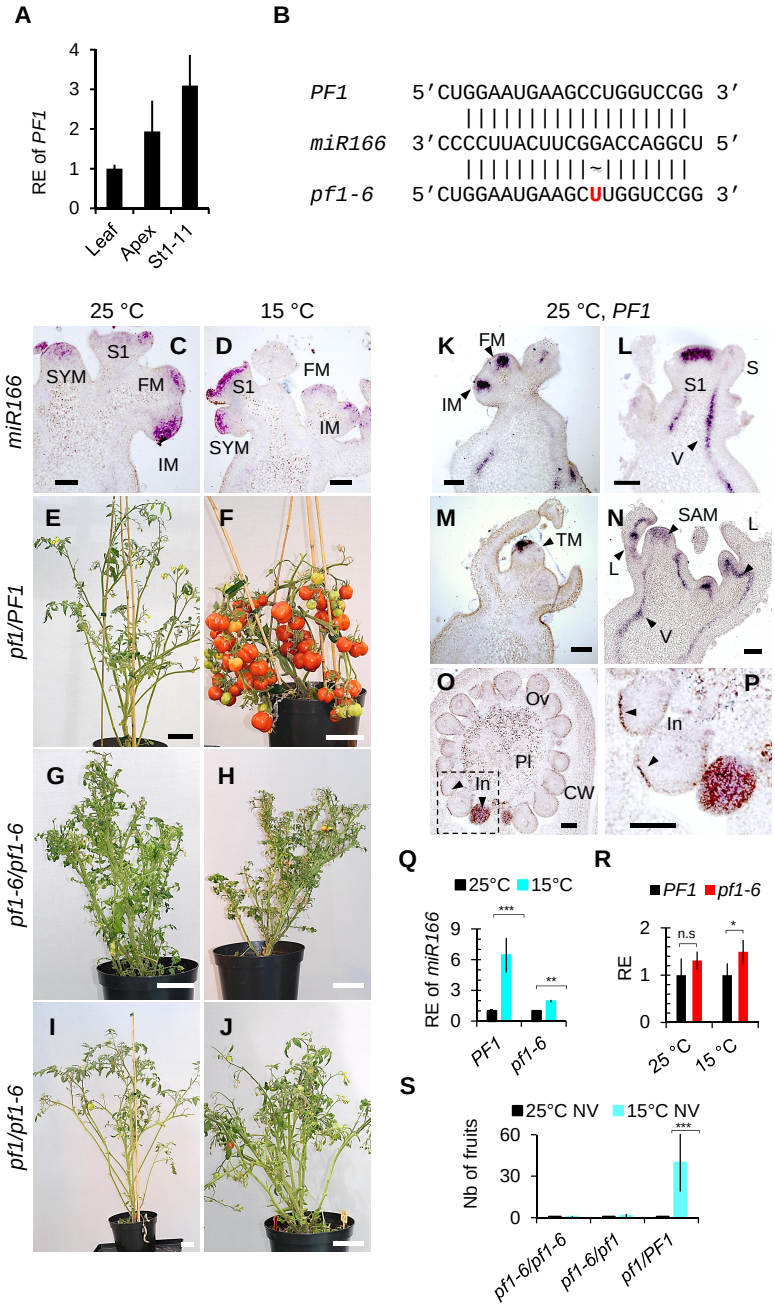
A
RE of PF1
Leaf
Apex
St1-11
B
PF1 5′CUGGAAUGAAGCCUGGUCCGG 3′
miR166 3′CCCCUUACUUCGGACCAGGCU 5′
pf1-6 5′CUGGAAUGAAGCUUGGUCCGG 3′
25 °C
15 °C
25 °C, PF1
miR166
pf1/PF1
pf1-6/pf1-6
pf1/pf1-6
S1
SYM
FM
IM
TM
SAM
V
Ov
Pl
In
CW
25°C
15°C
RE of miR166
PF1
pf1-6
RE
n.s
25 °C
15 °C
25°C NV
15°C NV
Nb of fruits
pf1-6/pf1-6
pf1-6/pf1
pf1/PF1

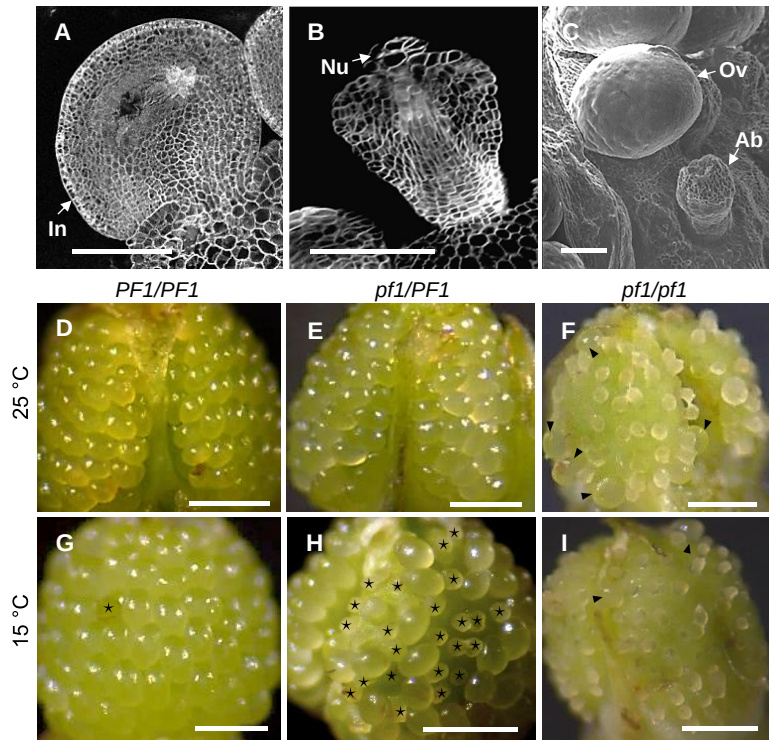

J

	25 °C day/ 18 °C night		15 °C day/ 12 °C night	
Genotype	Parthenocarpy	Aberrant Ovule	Parthenocarpy	Aberrant Ovule
PF1/PF1	No	0.4 ±0.7% a	No	0.3 ±0.4% a
pf1/PF1	No	0.1 ±0.3% a	Yes	51.1 ±17.7% b
pf1/pf1	Yes	91.3 ±0.9% b	Yes	95.4 ±0.9% c
pf1-3/PF1	No	0.3 ±0.4% a	No	0.4 ±0.7% a
pf1-3/pf1-3	No	0.3 ±0.4% a	Yes	20.4 ±5.1% d
pf1/pf1-3	No	2.9 ±1.3% c	Yes	83.2 ±8.4% e
pf1/pf1-6	No	0.3 ±0.4% a	No	0.3 ±0.4% a

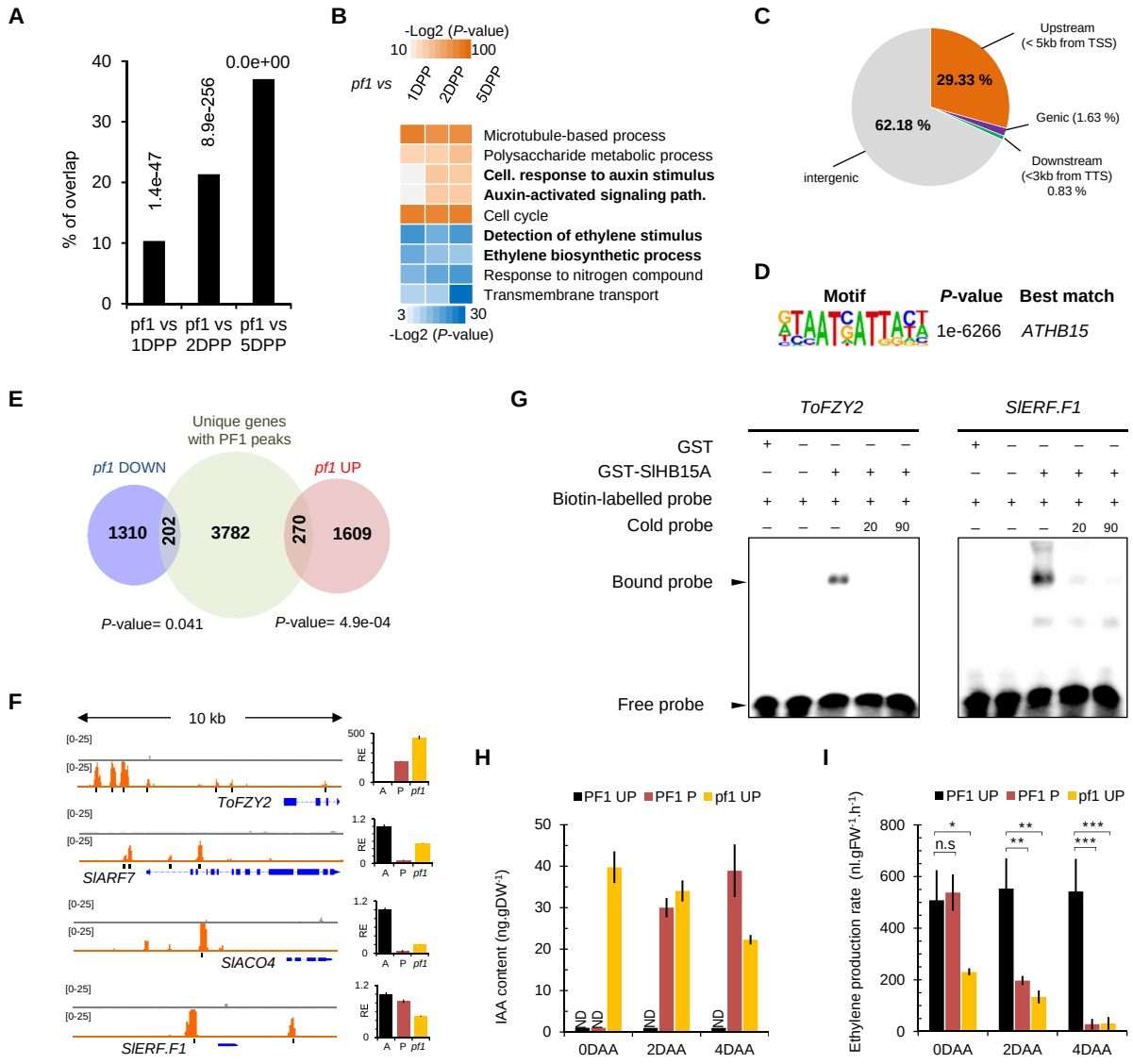
A
% of overlap
40
30
20
10
0
1.4e-47
8.9e-256
0.0e+00
pf1 vs 1DPP
pf1 vs 2DPP
pf1 vs 5DPP
B
-Log2 (P-value)
10
100
pf1 vs
1DPP
2DPP
5DPP
Microtubule-based process
Polysaccharide metabolic process
Cell. response to auxin stimulus
Auxin-activated signaling path.
Cell cycle
Detection of ethylene stimulus
Ethylene biosynthetic process
Response to nitrogen compound
Transmembrane transport
3
30
-Log2 (P-value)
C
Upstream
(< 5kb from TSS)
29.33 %
Genic (1.63 %)
62.18 %
intergenic
Downstream
(<3kb from TTS)
0.83 %
D
Motif
P-value
Best match
1e-6266
ATHB15
E
Unique genes
with PF1 peaks
pf1 DOWN
pf1 UP
1310
202
3782
270
1609
P-value= 0.041
P-value= 4.9e-04
F
10 kb
[0-25]
ToFZY2
SlARF7
SlACO4
SlERF.F1
RE
A
P
pf1
G
ToFZY2
SlERF.F1
GST
GST-SlHB15A
Biotin-labelled probe
Cold probe
Bound probe
Free probe
20
90
H
PF1 UP
PF1 P
pf1 UP
IAA content (ng.gDW-1)
ND
0DAA
2DAA
4DAA
I
PF1 UP
PF1 P
pf1 UP
Ethylene production rate (nl.gFW-1.h-1)
n.s
*
**
***
0DAA
2DAA
4DAA

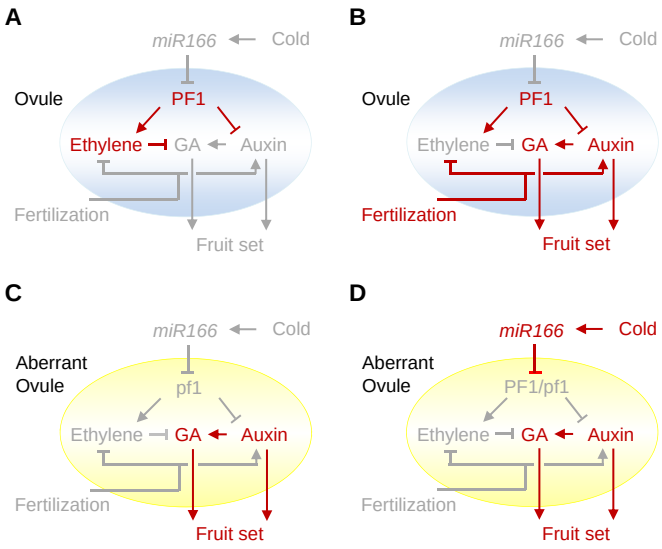
A
miR166
Cold
Ovule
PF1
Ethylene
GA
Auxin
Fertilization
Fruit set
B
miR166
Cold
Ovule
PF1
Ethylene
GA
Auxin
Fertilization
Fruit set
C
miR166
Cold
Aberrant
Ovule
pf1
Ethylene
GA
Auxin
Fertilization
Fruit set
D
miR166
Cold
Aberrant
Ovule
PF1/pf1
Ethylene
GA
Auxin
Fertilization
Fruit set